



Investigation of thermoforming processes of aerostructures: Simulation and microstructural analysis

Merve Çobanoğlu¹ · Remzi Ecmel Ece¹ · Büşra Ünlü^{1,2} · Yahya Öz¹ · Serkan Toros^{1,3} · Fahrettin Öztürk^{1,4}

Received: 4 October 2023 / Accepted: 12 April 2024
© The Author(s) 2024

Abstract

A series of experimental and numerical studies were carried out on the mechanical and geometric performance of an aerostructural part produced by a material out-of-autoclave stamp forming process using unidirectional (UD) carbon fiber (CF) reinforced polyetherketoneketone (PEKK), which provides advantages like reshaping, recycling, welding, and low serial manufacturing costs. As a novelty, initial part geometry, different types of springs, and their attachment type were examined experimentally and compared with simulations. Compression tests were performed to determine mechanical strengths which reach levels up to 550 MPa. In addition, differential scanning calorimetry (DSC) and thermogravimetric analysis (TGA) were conducted to determine the crystallinity which occurs depending on the cooling regimes of the material. The crystallinity has been observed to vary regionally ranging from 16 to 21%. However, the crystallinity of the part towards the cold mold region decreased from 20 to 17%. In addition, simulations were performed to observe and control the occurrence of wrinkles and other defects.

Keywords Aerospace applications · Crystallization · PEKK · Rapid manufacturing · Thermoforming · Thermoplastic

1 Introduction

CF reinforced thermoset (TS) matrix composite parts (CFRP) are widely desired due to their superior properties such as high strength/weight ratio, impact, and fatigue performance, damage tolerance, and high corrosion resistance [1–3]. These advanced properties are therefore commonly applied to aerospace structures. Consequently, carbon and glass fiber reinforced TS matrix composites have been widely used, especially for the Boeing 787 Dreamliner and Airbus A350. In both aircrafts approximately 50% of the structural weight are made up out of these composites [4, 5]. Contrarily to these advantageous properties of TS matrix

composites, major drawbacks are the emission of carbon dioxide (CO₂) caused by the energy required to process the material. Remarkably, CO₂ emission is regulated to a 75% reduction compared to the data from the Advisory Council for Aviation Research for the year 2000 [6–8]. Additionally, important disadvantages of TSs are that it is not possible to reshape, recycle, weld or post-process due to the network structure of TSs after the autoclave process performed under high temperature and pressure. In addition, TS matrix composites require a clean room for decreasing contaminations while the manufacturing time is increased due to long curing cycles. Moreover, the lifetime of TS resin impregnated CFs (prepregs) is limited and needs refrigeration. Therefore, thermoplastic (TP) matrix CF reinforced composites can replace TS matrix composites since unfavorable properties of TSs are not available due to reshapability, formability, recyclability, and weldability properties of TPs [9, 10]. Moreover, fusion joining and additive manufacturing approaches are applicable [11–13].

Among these advantageous properties of TPs, the most important one is the improved toughness, since TPs have a branched or linear structure. Moreover, strong covalent bonds and weak secondary bonds (van der Waals) exist between chains, and thus, improved crystallinity exists

✉ Serkan Toros
serkantoros@ohu.edu.tr

¹ Turkish Aerospace, 06980 Ankara, Turkey

² Department of Metallurgical and Materials Engineering, Middle East Technical University, 06800 Ankara, Turkey

³ Department of Mechanical Engineering, Niğde Ömer Halisdemir University, 51240 Niğde, Turkey

⁴ Department of Mechanical Engineering, Ankara Yıldırım Beyazıt University, 06010 Ankara, Turkey

which results in enhanced damage tolerance [14]. When heated or dissolved by a solvent, secondary bonds are easily broken. Therefore, TPs can be re-softened, reformed, re-used, or recycled. Additionally, since TPs are fully reacted, they do not require any reaction during the consolidation process. Thus, TPs can be consolidated in a manner of short time compared to TSs curing cycle. Moreover, TPs show high durability under thermal conditions which improves the thermal stability under supersonic and high-temperature conditions while fire retardancy properties of TPs are used especially in nacelles [15–18]. Due to these advantageous properties, research of TP composites has been accelerated enormously [19–21]. This evolution resulted in large-scale production studies for the transportation field leading the way for the aerospace industry [20, 22, 23].

Within the scope of this study, the matrix material was chosen from the poly(aryl ether ketone) (PAEK) family where ether groups are bonded with ketone groups. The amount of ketone groups affects the melting temperature of TPs. Increased durability under high temperature, high strength to weight ratio and resistance to corrosion make them suitable for aerospace applications. Additionally, since the PAEK group is semi-crystalline, the failure mechanism of the polymer is convenient for primary parts of aircrafts. The most exceptional mechanical and thermal performance in the PAEK family is exhibited by PEKK [24–27]. Furthermore, crystallization kinetics [28, 29], crack propagation properties [30], and effects of the fiber–matrix interface on mechanical properties [31] were also studied in the literature.

Thus, PEKK was used as matrix material in CF reinforced composites in this study. The manufacturing process included preheating, thermoforming, and consolidation. During the thermoforming process, main mechanisms of manufacturing include percolation of polymers via matrix flow through layers, transverse flow under pressurized condition fibers, and intraply shear during the forming operation. This process is advantageous for large-scale production since the cycle time is very low compared to TSs. The thermoforming process requires pre-consolidated plates for manufacturing. Therefore, autoclave consolidation of prepregs under high temperature and pressure was used for this process [6, 32, 33].

The manufacturing process was simulated concurrently. The formability of CF reinforced TP (CFRTP) composites was analyzed and simulated by AniForm in this study. Improved accuracy and lowering simulation times are the most important parameters for the analysis.

Thus, within the scope of this study, an aerostructural part was manufactured by a material forming process applied on CF reinforced PEKK. Part geometry, different types of springs and their attachment were studied by simulations and compared with the obtained aerostructure.

Table 1 Polymer matrix properties

Matrix properties	Value
Density	1.30 g/cm ³
T_g (glass transition)	160 °C
T_m (melting temperature)	337 °C
T_C (crystallization temperature)	265 °C
T_p (processing)	370–400 °C

Table 2 Carbon UD tape (semipreg) properties

Carbon UD tape (CF+resin) properties	Value
Density	1.59 g/cm ³
Polymer content by weight	34%
Consolidated ply thickness	0.14 mm
Tensile strength 0°	2410 MPa
Tensile strength 90°	86 MPa

In addition, mechanical and thermal tests were performed. Moreover, effects of the crystallization occurring during the manufacturing process were investigated.

2 Materials and methods

2.1 Raw material properties

Toray Cetex TC1320 PEKK is a high-quality TP composite material that employs the semi-crystalline TP polymer PEKK for superior elevated service performance. It has high mechanical properties as well as good hot/wet strength. The semi-crystalline structure of the polymer matrix assures that it is very resistant to chemicals and solvents, while having outstanding flammability capabilities. In addition, Toray Cetex TC1320 is qualified and certified for aerospace applications. Tables 1 and 2 summarize physical and mechanical properties of the polymer and tape, respectively.

2.2 Pre-consolidation process of blanks

Blanks used for thermoforming were cut from pre-consolidated laminates such that ply cutting and ply orientation processes were executed first. Blanks were manufactured by consolidating imbricated 14 unidirectional PEKK plies which have been orientated in different directions as [45°, 0°, 90°, –45°, 90°, 0°, 45°]_s. For the purpose of reducing void formation and delamination, an autoclave was preferred for the consolidation operation. Prior the consolidation operation, the hand lay-up process was conducted in a clean room to minimize contamination. After vacuum bagging, a stack of oriented plies started to melt at 380 °C under 8 bar

in an autoclave for 2 h. Figure 1 depicts the bagging scheme while it also presents the time/pressure–temperature diagram of the autoclave cycle. In order to obtain the final shape, a water jet cutting machine or guillotine press can be operated.

2.3 TP composite forming process and heat management

2.3.1 Heat management of the composite forming

It is possible to shape carbon/glass fiber reinforced TP matrix composites using the stamp forming method. While materials with polymer matrices are subjected to the forming process, they need a higher heating temperature and pressure in comparison to pure polymer materials. Generally, forming processes of TP composite sheets consist of several stages. These stages include (i) fixing the polymer matrix composite laminate to the movable frame by holders (bolted union with springs per hole), (ii) heating the laminate until it reaches the required temperature to become formable for the stamp forming process, (iii) closing matched dies and initiating the cooling of the laminate, and (iv) demolding and trimming processes.

Basic process steps and temperature variations for the whole procedure are illustrated in Fig. 2. Since the mid-section is the coolest part during heating, it is important to follow heating at these locations. Radius parts are also

critical. Therefore, three thermocouples were placed (i.e., two of them at the radius, one of them at the middle of the part). TP composite sheets were heated for approximately 240 s with a ceramic heater up to 380 °C. Afterwards, sheets were transferred within a short time to the die system which was already heated. Subsequently, the dies closing operation followed. Finally, dies were held in a closed position to heat TP composite sheets for a specific time period as indicated in Fig. 2.

Dies (prepared by use of the material DM3X which exhibits a low coefficient of thermal expansion) have to be at consolidation temperature during the stamping process, i.e., approximately 230–250 °C for PEKK matrix composites. Remarkably, there are various ways to heat up tools such as infrared, induction, and thermal fluid heating. In this study, composite parts were formed with tools heated by thermal fluid heating. In order to keep the consolidation temperature steady, the tooling enclosure was insulated with glass wool. Also, 25-mm-thick mica insulation plates were placed between the tools and press ram table for reducing heat loss by conductive heat transfer. According to measurements of temperatures on the die system, male and female tools were warmed up by a heating boiler to form melted blanks at crystallization temperatures between 227 and 249 °C. The die heating channels' positions and flow rate of the heating fluid were calibrated to minimize the temperature gradient through die surfaces. Stamp forming was executed under

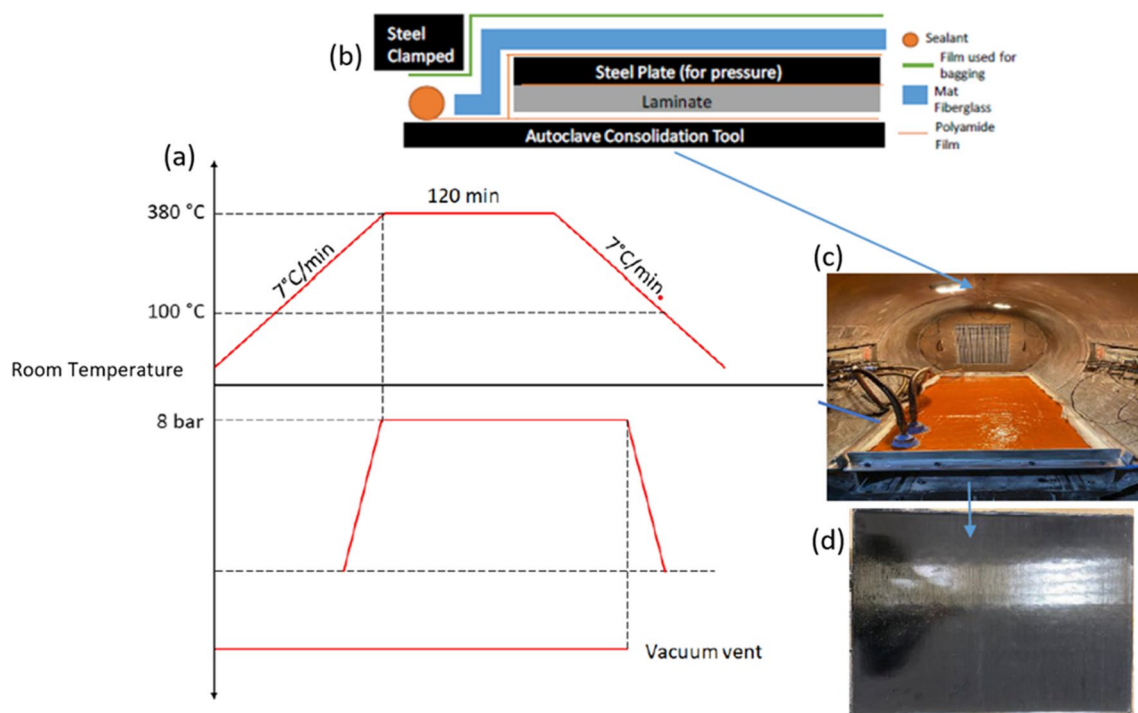
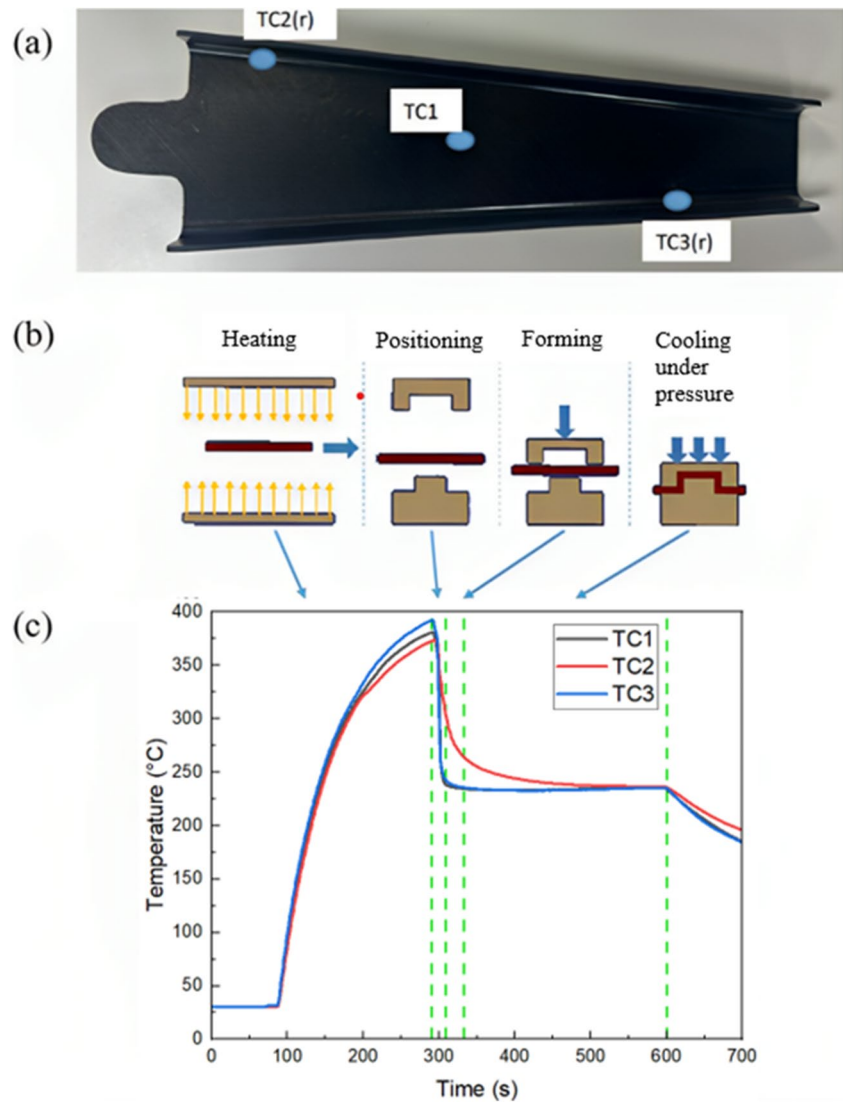


Fig. 1 a Time/pressure–temperature diagram of the autoclave cycle. b Lay-up of the corresponding vacuum bagging c in an autoclave and resulting d consolidated TP sheet

Fig. 2 a Thermocouple locations, where r indicates the radius, b basic process flow, and c corresponding time/temperature diagram



195 bar hydraulic pressure for approximately 2 min. To cut up excess material, the bench trimmer process was applied.

In Fig. 3, the design image of the composite forming experimental setup is shown. Here, composite sheets are transported between stations by a conveying system controlled by servo motors. Firstly, the composite plate placed in the frame is transported to heaters and kept there until the desired temperature level is reached. Afterwards, it is quickly applied to the die system and the forming process is completed. By choosing the closing speed of the dies as fast as possible, the heat loss in the composite plates are minimized. After the last baking molds are completely closed, they are kept under high pressure to consolidate the part.

2.3.2 Gripping of the blank

One of the essential parameters that affect the quality of the formed TP composite sheet is the fixing methodology.

The general application at the stamping operation is the fixing of sheets with the help of springs instead of the secondary die system, i.e., the blank holder system. During the closing of the male and female dies, blank holders may prevent sliding of the sheets. This phenomenon may lead to separation between fibers particularly for UD composites. According to the final product design, initial positions and amounts of springs as well as their stiffness are critical parameters to obtain well-formed parts without any defects like wrinkling, folding, and separations [34]. Bolted-union grippers, metal grippers, and springs can be used to attach the blank to the frame of the mechanism. In addition to the gripping system, the initial blank geometry also needs to be studied to obtain flawless parts. In this study, in terms of length and stiffness, four different springs were used to hold composite sheets. Figures 4 and 5 present different fixations of the blanks that were cut in complex and rectangular shape, respectively.

Fig. 3 Picture of experimental setup

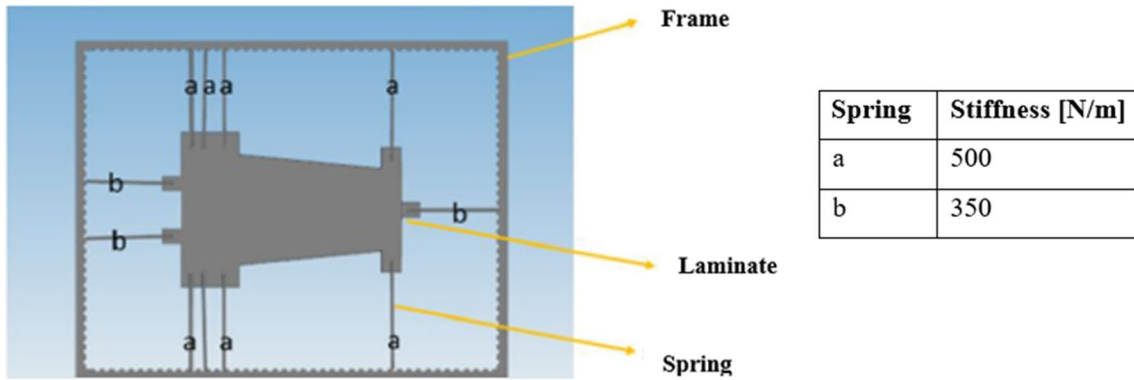
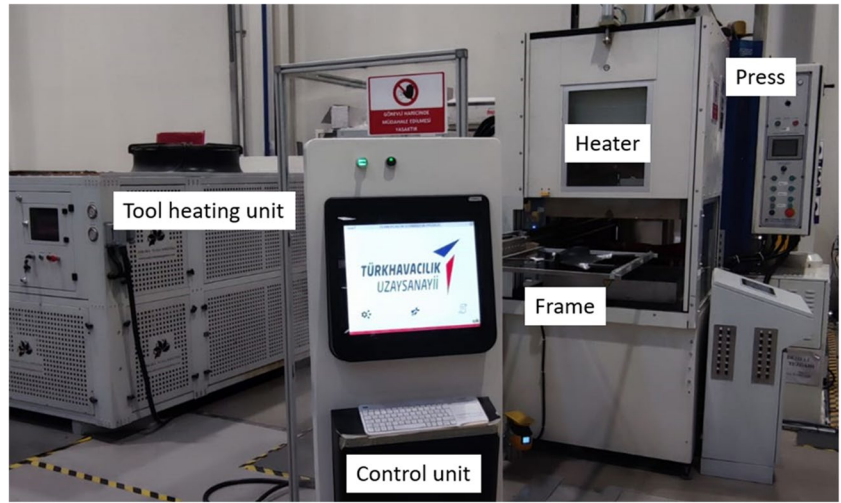
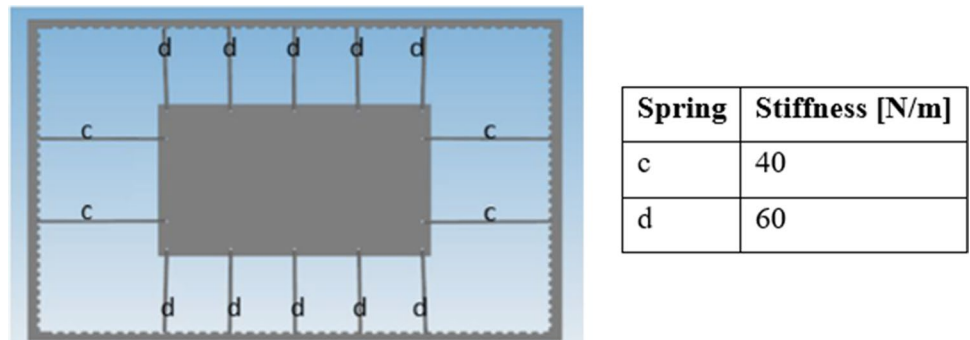


Fig. 4 Complex geometry, setup-A

Fig. 5 Rectangular geometry, setup-B



2.4 Numerical modeling of the stamping operation

The commercially available AniForm software, which is specialized on stamp forming simulations of composites, was used. Besides the springs definition (amount of springs and their stiffness) for the fixing of composite sheets, the software performs forming simulations under non-isothermal conditions in which heat is transferred between composite sheets and forming tools. This feature also allows the

determination of the crystallinity in the material depending on the time. The composite forming simulation used the applicable Nakamura model which indicates non-isothermal kinetics [35, 36]. Since the Avrami assumption is only valid for instantaneous growth after activation and uniformity of the germ location as well as given crystal growth morphology and isothermal crystallization conditions, Nakamura developed the integration of non-isothermal crystallization of polymeric materials [35–37]. The corresponding equation

is presented as Eq. (1), where $K(T)$ is the Nakamura kinetics crystallization function at temperature T and $\alpha(t)$ is the degree of phase transformation at time t .

$$\alpha(t) = 1 - \exp\left(-\int_0^t K(T)d\tau\right) \quad (1)$$

Since PEKK is a semicrystalline material, Nakamura extends the Avrami model for non-isothermal cases while the degree of crystallization is identified by this method [35, 38].

Simulation models were created by importing surface models of dies, frames, and blanks such that the timeframe of analyses was minimized and the process was accelerated. In the carried out simulations, corresponding to the experimental system, the frame was first moved down to 52 mm and the composite plate was placed on the male mold. Afterwards, the female mold was closed with a speed of 300 mm/s and a pressure of 195 bar was applied on the plate. The temperature, which is another important forming process parameter that depends on the geometry of tools and heating methodology, can vary across die surfaces. However, since the software capability is not appropriate for reflecting this variation, simulations were carried out under constant 260 °C in accordance with the temperature during the forming as observable in Fig. 2. Another important key point in the simulations is to obtain equivalent results with the experiment. Therefore, properties such as heat conduction and friction between mold surfaces and composite plates can be defined as material properties while similar characteristics between composite layers can also be prescribed. The friction coefficient in the composite layups was taken as 0.2 while 0.25 was chosen for the forming tools and composites upper as well as lower surface. In addition, to characterize the permanent forming behavior of the composites, several mechanical tests are required. Required experimental findings like bias-extension characteristics at different temperatures, in-plane shear characterization which is obtained from torsion tests and/or picture frame tests, can be fed to the software. Relevant data were obtained from the manufacturer of Toray Cetex TC1320 PEKK, Toray Industries.

The material behavior in the simulations is composed of combined fiber and matrix deformations. The deformation of the matrix is defined by a cross-flow formulation which is the shear rate dependent viscosity model. The corresponding Cauchy stress σ can be expressed by Eq. (2):

$$\sigma = \frac{2\eta(\dot{\gamma})}{J}D, \quad (2)$$

where η is the viscosity which depends on the equivalent shear rate $\dot{\gamma}$, J is the Jacobian of the deformation gradient, and D is the rate of the deformation tensor. Correspondingly, the shear rate viscosity is provided by Eq. (3):

$$\eta(\dot{\gamma}) = \frac{\eta_0 - \eta_\infty}{1 + m\dot{\gamma}^{1-n}} + \eta_\infty, \quad (3)$$

where η_0 and η_∞ are viscosity values at specified minimum and maximum shear strain rate values which are experimentally obtained. m and n are material constants that control the model fitting performance. In the simulations, $\eta_0 = 4.84$ Pas, $\eta_\infty = 0.29$ Pas, $m = 135$, and $n = 0.046$ were used.

According to a myriad of analyses and experimental studies [39], two simulation models were run in detail as can be seen in Fig. 6. Hence, setups presented in Figs. 4 and 5, i.e., positioning of the springs, were tested and compared by AniForm.

2.5 Characterizations

As can be observed in Fig. 7, test samples were cut by a waterjet for the purpose of observing selected regions with regard to effects of the forming operation and process parameters. In this research, compression tests were applied to samples obtained from the sheet before the thermoforming operation and from the RIB part which was formed in order to determine and compare their mechanical properties. A servo controlled Instron 5985 tensile/compression test machine was utilized for these measurements. Deformations were measured by strain gauges which had a resistance of $350.0 \pm 0.2 \Omega$ with a 2.125% gauge factor at room temperature. The compression test speed was selected as 1.3 mm/min as described in the ASTM D6641 standard while samples were prepared accordingly. For thermal analyses, $1 \times 1 \text{ cm}^2$ samples were obtained from specific points depicted in Fig. 7 and labeled as DSC1–DSC6 by scraping the polymer from the resulting surface. DSC analyses were performed to determine the crystallinity of the composite [40]. In this study, the weight of DSC samples was approximately 10 mg. Measurements were performed with a heating rate of 10 °C/min under nitrogen flow while aluminum pens were used. Remarkably, the amount of amorphous and crystalline regions of the material provides information about the quality of the TP composite. Furthermore, during DSC, glassy and melting temperatures of the samples were

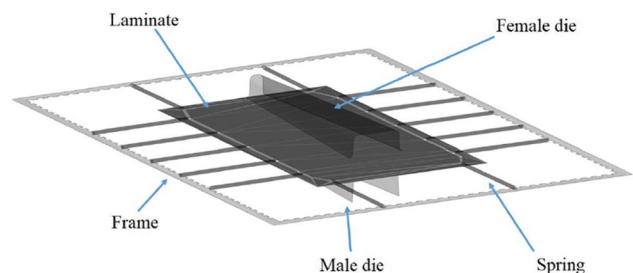


Fig. 6 TP composite forming simulation

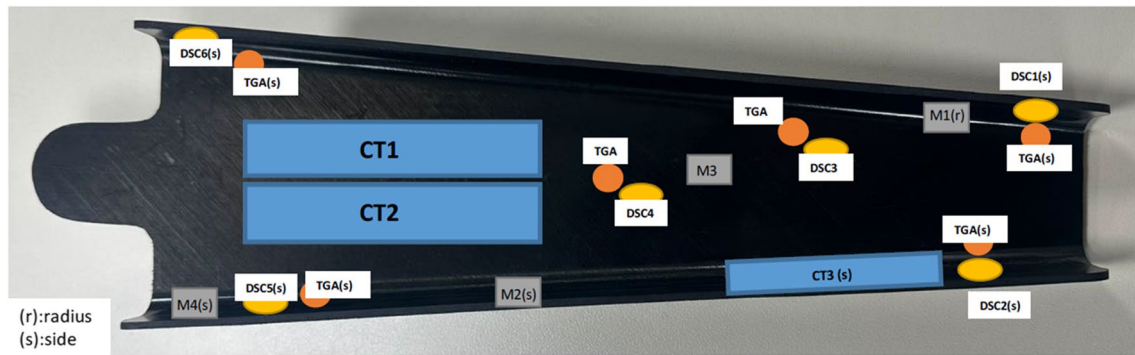


Fig. 7 Selected regions of the RIB for characterization tests. M1–M4 are used for microscopic analyses while CT1–CT3 are utilized for compression tests

also observed. For this analysis, a Perkin Elmer Diamond DSC device was used and crystallinities of the samples were determined according to the ISO EN11357 standard. In addition to the DSC analysis, TGA which is another critical thermal analysis technique for studying TP composites was applied on different samples labeled as TGA1–TGA6 as indicated in Fig. 7 by use of a TA Instruments Q500 with a heating rate of 10 °C/min under nitrogen atmosphere. The approach provides information about physical properties of the material such as decomposition and thermal stability. Within this regard, TGA was performed on the composites before and after the stamp forming. In addition, micro-cut characterization is an important technique for considering the quality of materials. Void amount, fiber–matrix bond quality, and thickness distribution of the formed part are essential parameters which are required to be analyzed in an optic microscope. Microstructure images of the RIB part and the blank were prepared based on classical metallographic methods (cutting-grinding-polishing). Critical regions of the RIB part were selected. An Olympus GX-53 Inverted Microscope was used for this purpose. Scanning electron microscopy (SEM) was carried out using a FEI Quanta 200 FEG device. Samples were coated with a gold/palladium thin film before examining the microstructure.

3 Results and discussion

3.1 Mechanical and thermal properties of the aerostructure

Characterization of mechanical properties of TP composite materials to be used in structural parts of aircrafts requires a number of mechanical tests.

As can be seen in Fig. 8, samples that are taken from formed RIB parts have higher strength than consolidated sheets prior forming operations which was measured as

330 MPa lying slightly lower than the value of 337 MPa provided by the manufacturer. This observation occurs due to reduced voids as well as pores, strain hardening, and increasing density, which arise through the stamp forming process [41]. As a result of the measurements, chord module (slope of the curves) values of the parts were also determined. The chord modulus values of the CT1 and CT2 samples in the upper plane of the shaped part were calculated as 44.08 and 45.94 GPa, respectively. However, this value was determined as 46.09 GPa for the CT3 sample which was placed on the side of the aerostructure. Calculations were performed from the compressive strain between 1000 and 3000 $\mu\text{m}/\mu\text{m}$ as depicted in Fig. 8. One of the essential features of TPs is the controlling of mechanical properties via heating and cooling regimes. Selected conditions for tools like temperature, forming speed, and/or transferring period of sheets affect crystallization kinetics and its ratio in the microstructure. In order to determine this relation between strength and crystallization, DSC and TGA tests were applied to the sheet

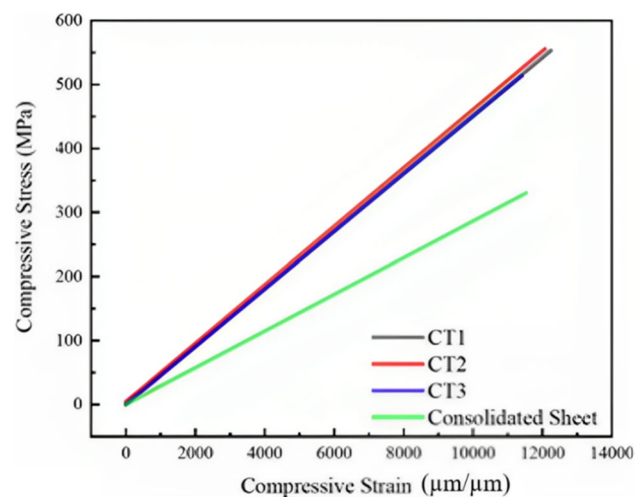


Fig. 8 Compression test results of test samples taken from the part

(before the thermoforming operation) and RIB part (after the thermoforming operation) to determine and compare their properties. Note that the RIB part is a standard aerostructure used as a forming element of wings.

There were a number of noteworthy results observed when DSC results of the RIB parts were studied. The thermoforming operation does neither change polymer nor fiber content. Therefore, it can be concluded that the thermoforming operation was successful with regard to the material. Additionally, crystallinity is a critical parameter for TP composites since it provides a general opinion about the process. Before the thermoforming operation, the blank has some crystallinity; however, when the TP composite reached the process temperature range, polymer chains move more freely reducing intermolecular forces. While under pressure, polymer chains come into close contact, promoting intermolecular bonding between them. Afterwards, during cooling under the tool, polymer chains lose their mobility, and as a result, the material solidifies and retains the shape of the mold [42]. Correspondingly, the crystallinity of the TP demonstrates the reliability of the thermoforming process [43]. Moreover, these bonds provide enhanced mechanical strength and toughness. Thus, DSC analysis provides indirect information about mechanical properties of the material.

When Tables 3 and 4 are examined, it can be observed that the crystallinity of the PEKK RIB composite is nearly 20% while this value is lower in certain regions as shown in Table 3. Note that the contact pressure of the RIB part during forming differs throughout the radius and web surface parts such that this difference may cause variations in the crystallinity. These observations are also supported with void amounts observed in microstructure images (as presented in Section 3.2) since the crystallinity of the TP decreases with increasing void amounts which shows that these results are consistent. Considering Table 3, the maximum crystallinity reaches up to 20.33% for the DSC5 point measured from the top surface of the samples whereas the minimum crystallinity was determined as 16.53% from the DSC6 sample located at the side. A significant parameter which affects the crystallinity ratio is the cooling rate of the parts during the forming operation. It is well known that the crystallinity decreases with increasing cooling

Table 4 DSC results of the RIB through the thickness

Region	Resin content (%)	T_g (°C)	T_m (°C)	Crystallinity (%)
Top	34	157.9	330.6	20.0
Middle	34	155.2	329.6	17.4
Bottom	34	157.0	328.2	17.2

rates for some TP polymers [44]. This situation can only occur when the temperature between tool and TP composite is relatively high. As aforementioned, the tools' temperature can variate from inletting the heating fluid to the outlet. This leads to a crystallization variation in the TP composite parts [44]. The cooling rate can also variate due to the thermal conduction which is affected by the applied force (contact pressure) on the samples. Generally, the contact pressure on the side walls of the samples is less than the flat regions of the dies. Therefore, it is expected that the cooling rate is much higher for flat regions in comparison to the side walls due to the contact pressure effect [44]. Furthermore, the glass transition temperature in Table 3 is comparable to Table 1 while the melting temperature is slightly decreased.

Another important aspect about quantities supplied from the RIB part is the determination of the crystallization ability of the part along its thickness. As mentioned before, especially in the forming processes of TP composites, differences between mold temperatures and ambient temperature as well as temperature differences between mold systems significantly affect these crystallization values. This can lead not only to crystallization rates on selected planes but also to different values in their crystallization along the thickness [43]. In Table 4, crystallization ratios along the thickness of the DSC4 sample, which are in agreement with this argument, are presented. After the polymer was excavated from upper and lower surfaces, they were divided into two pieces with approximately the same thickness throughout the part thickness.

TGA results are presented in Table 3 and Fig. 9. Before stamp forming negligible weight losses until 400 °C occur, implying that all volatiles evaporated during the

Table 3 DSC and TGA results of the RIB. $T_{d,5\%}$ and $T_{d,max}$ represent temperatures at 5% and maximum weight loss, respectively

Sample	Resin content (%)	T_g (°C)	T_m (°C)	Crystallinity (%)	$T_{d,5\%}$ (°C)	$T_{d,max}$ (°C)	Char yield (%)
DSC1	34	158.1	330.7	19.3	568	573	13.4
DSC2	34	158.5	331.6	18.3	565	571	13.1
DSC3	34	152.4	330.7	21.2	564	570	13.0
DSC4	34	155.3	330.5	20.0	567	576	15.8
DSC5	34	160.3	329.7	20.3	570	577	13.3
DSC6	34	158.5	329.7	16.5	568	576	13.5

consolidation of the sheet in the autoclave. Results also show that samples exhibit a one-step degradative behavior which was also revealed by a derivative thermogravimetric (DTG) analysis presented in Fig. 9b. A characteristic mass release of about 15% takes place which starts at 510 °C and ends at approximately 710 °C which is an indication for the high thermal stability of this TP in contrast to TS matrices [45]. This process might start with the rupture of the weakest bonds amid aromatic groups while the major volatile release might contain phenol [45, 46]. After the stamp forming process, it can be observed that temperatures at 5% and maximum weight loss are slightly decreased while the char yield

increased. However, no correlation between the location of the samples and TGA results is detectable.

3.2 Micro-cut analysis of specified regions

Micro-cut analysis results are presented in Figs. 10 and 11. As can be observed, voids caused by separation between layers, trapped air bubbles during the laying and the autoclave process or fiber folding during the shaping are quite rare. The void amount was determined to lie between 0.82 and 1.46% while the maximum void length was 0.15 cm.

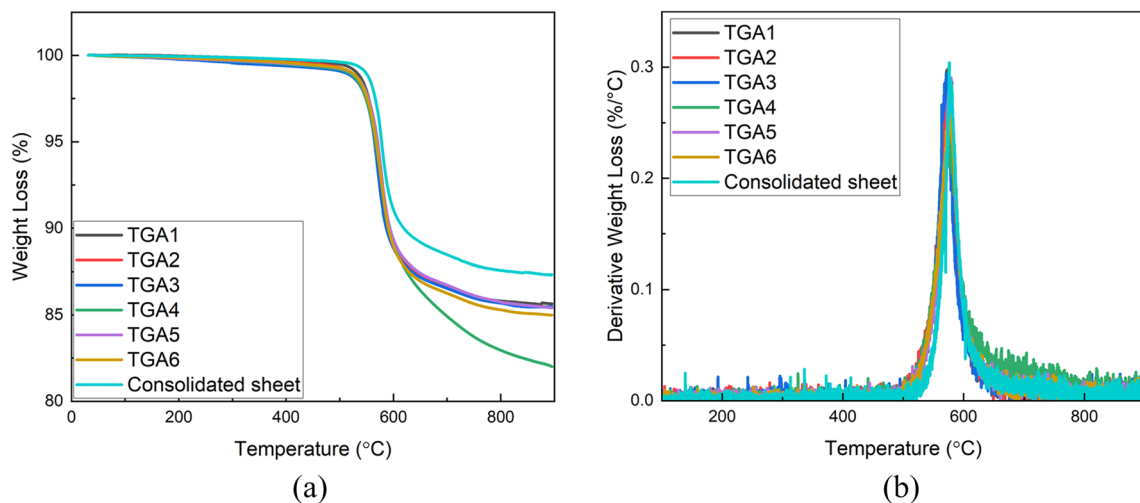


Fig. 9 a TGA and b DTG results before and after stamp forming

Fig. 10 Microstructure images of different regions of the RIB part

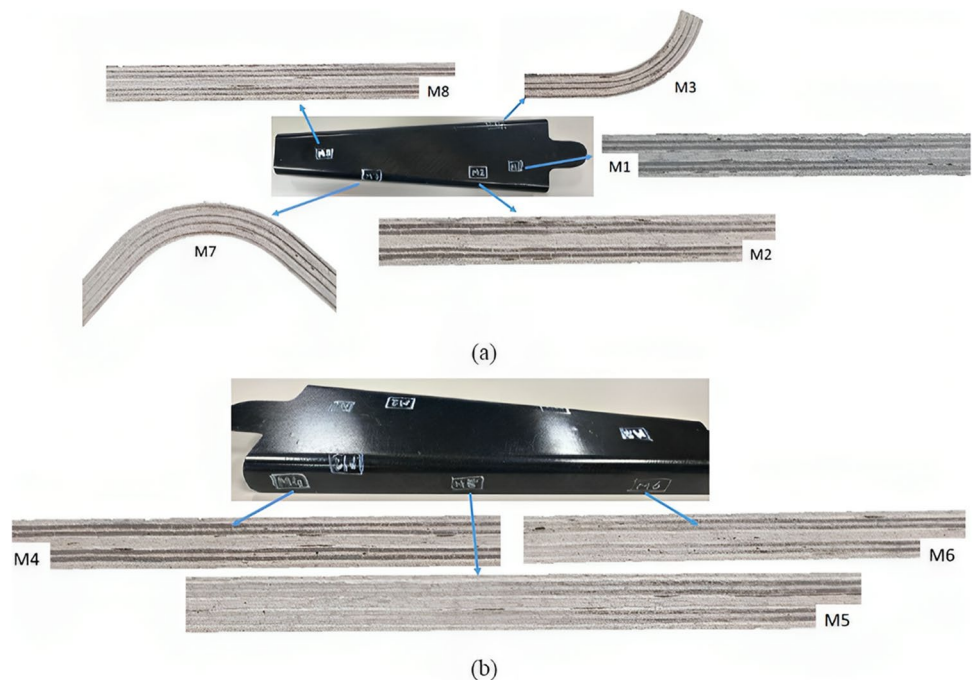


Fig. 11 Regions a M3 and b M7 located at the radius for which thicknesses were measured

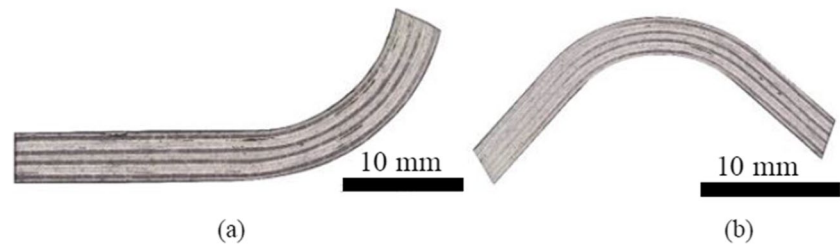


Table 5 Thickness measurement results

Thickness (μm)	T1	T2	T3	T4	T5	T6
M1	2024.03	2034.59	2041.60	X	X	X
M2	2016.97	2027.57	2020.68	X	X	X
M3	1920.94	1915.76	1896.81	1951.45	2001.15	2006.60
M4	1999.42	1994.09	2008.22	X	X	X
M5	1995.95	1995.89	1992.37	X	X	X
M6	1980.00	1983.57	1971.35	X	X	X
M7	2040.12	1986.66	1963.34	1947.06	1985.06	X
M8	1920.21	1909.63	1899.11	X	X	X

Another important parameter of the forming process of TP parts is the thickness distribution in the parts. Especially in the stages of bringing complex geometries such as edge bending and curvature to the part, it is a serious challenge to obtain a homogeneous thickness distribution due to the properties of the part at relevant temperatures. In this sense, a different approach has to be used in comparison to die tolerances used in routine sheet metal forming processes. Die tolerances are a matter of precision in order to avoid formation of previously mentioned defects in the composite, which expand under the influence of heat and transform into fluid form. According to the carried out measurements, thickness distributions of formed parts of specified regions are complying with blank and tool tolerances. Hence, the forming operation was successful with regard to the visual aspect. Results of the thickness measurements are presented in Table 5. Thickness measurements were performed at three different regions with the exception of M3 and M7 since both regions are located at the radius. Therefore, more measurements were performed for these locations as depicted in Fig. 11. In addition, Fig. 12 presents an exemplary SEM image of the M3 radius for higher resolution purposes where varying UD PEKK plies and no voids are discernible.

3.3 TP composite forming simulation results

The use of qualified software for the evaluation of TP composites' forming processes in a computing environment is of great interest [47]. In modeling studies developed similarly for sheet metal forming processes [48], it is of major importance to define material properties for forming

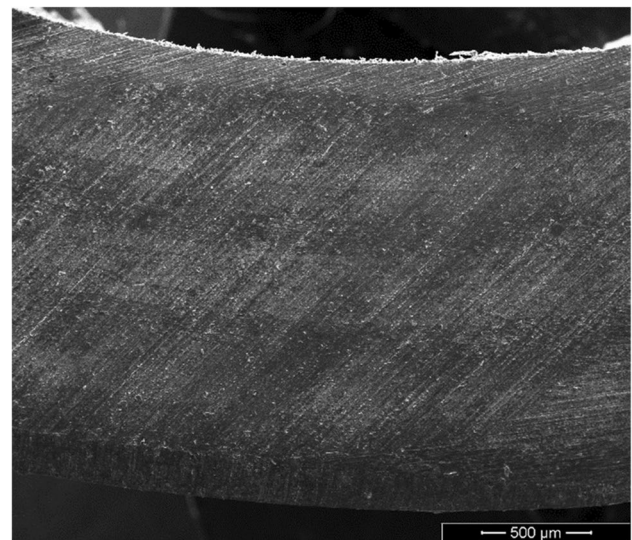


Fig. 12 SEM image of M3

simulations. Studies are carried out in the literature, especially in software such as LS-DYNA, Abaqus FEA, Pam-Stamp, and AniForm. In this study, AniForm developed directly for composite forming processes was used. Performance comparisons of the relevant software are available in the literature. Results show that AniForm provides an enhancement in estimating dimensional properties for the fixed part as mentioned in the literature [49].

In this present research, firstly, suspended studies were carried out with the initial plate geometry and springs, which directly affect final dimensions of plates shaped in TP composite forming processes and defects such as wrinkles. These

properties are ultimately adjusted according to the geometry of the part to be produced while each region must act in a controlled manner at the point of filling the material into the mold during the forming. In addition to the starting part shape, connection points of relevant springs and the stiffness of used springs also play an important role. Note that the two different part geometries and the used connection method within the scope of this study were described in Sections 2.3 and 2.4.

Geometric results of the forming simulations applied for the PEKK TP composite are presented in Fig. 13. As can be observed, although there is no complication in the upper plane areas with regard to wrinkles, minor wrinkle lines on the side walls and/or closest regions to side walls occur in the simulations for the full rectangular part (setup-B). These wrinkles are obtained in accordance with inhomogeneous pulls in each region during the filling of the material inside the mold. Moreover, the design in which geometric dimensions after the shaping matched design dimensions was also obtained from the initial part geometry given in Fig. 13.

The wrinkle problem is one of the most significant complications encountered in the shaping of TP composites. This situation mostly occurs in two different ways. One of them is in the form of significant fluctuations on the surface

of the part, while the other occurs in the folds formed by the material thickness of CFs. This has a significant impact on the quality of the final part and necessitates that fiber orientations must be taken into account when the part is filled into the mold. When wrinkle values of the two shaped geometries are examined as depicted in Fig. 14, it is observable that the wrinkle tendency is less in the part with a full rectangular section (particularly in the bending areas).

Another important feature to be observed in the performed shaping simulations is the observation of possible separations between layers of the composite sheet. In general, these decompositions can be observed in parts if fiber wrinkles exceed a certain critical value. This situation is directly dependent on the thickness of the layer related to the fiber and matrix ratio in the initial case. When wrinkle-level behaviors presented in Fig. 14 and the layer separation tendency distributions shown in Fig. 15 are evaluated together, it is obvious that the relevant error is an expected result. It can be foreseen that wrinkles and related layer separations (delaminations) may occur especially in negative-angled wall parts. Moreover, they affect each other. However, in the analyses, it is observable that the distribution of defects depends on the initial part geometry. Remarkably, involved defects are less achieved in the flat rectangular part.

Fig. 13 Isometric views of simulations

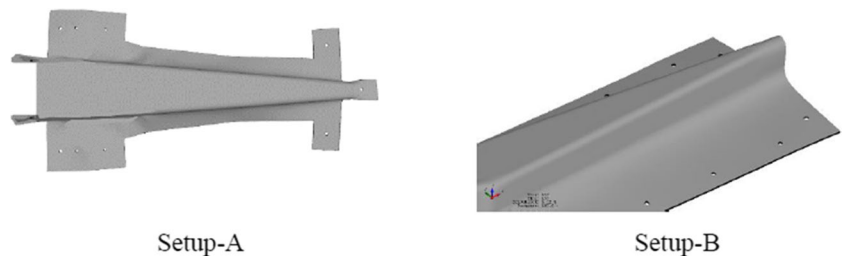


Fig. 14 Wrinkling intensity of the formed parts

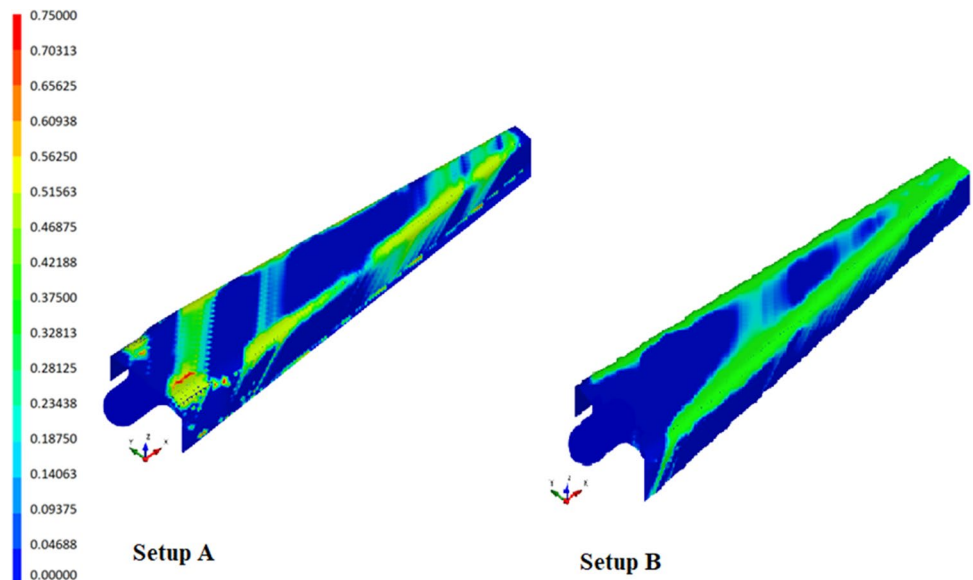


Fig. 15 Ply splitting intensity

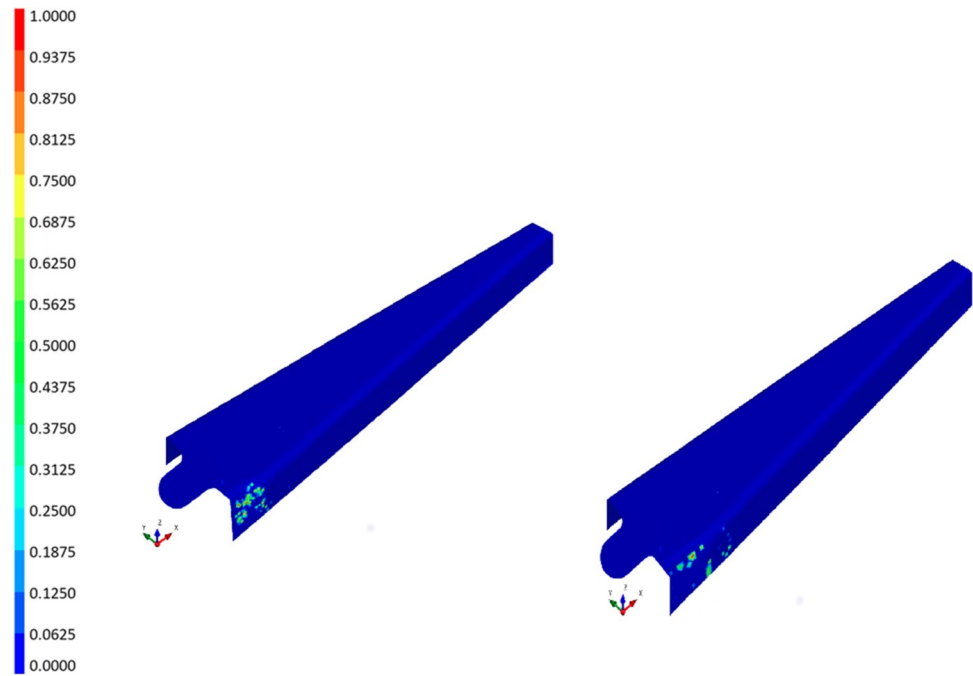


Table 6 Summarized results of stamp forming TP composites

Advantages	Disadvantages
Strength increases after stamp forming according to the crystallization	Crystallinity might be decreased at side walls due to different cooling rates and insufficient pressures
High thermal stability	Wrinkles might occur at side walls and corners
Short cycle times for manufacturing	Delamination may occur in negative-angled parts
Easy one-step forming of complex shaped parts	High-quality surface finishes can sometimes be challenging due to high temperature requirements

4 Conclusion

A series of experimental and numerical studies were performed on the forming processes of TP composites. Providing a systematic approach yields structural parts which fulfil mechanical as well as geometric design requirements. Corresponding exemplary results were presented for a RIB part of an aircraft. Simulations revealed that under certain circumstances (for instance, negative-angled wall parts) wrinkles and delamination can occur. As a result, these situations could be avoided in the aerostructure presented in this study. Table 6 provides a summarized overview.

Moreover, typical drawbacks like buckling, fiber breakage, or resin migration did not occur due to the chosen process parameters, i.e., stamping pressure and velocity. In contrast to many previous studies [38], UD composites were used in this work which are in general more prone to wrinkling.

Nevertheless, wrinkling was avoided. Moreover, compression levels up to 550 MPa were determined. In addition, crystallinity which affect mechanical properties has been observed to vary regionally ranging from 16 to 21%. Hence, advantages of TP composites (recycling, reshaping, out-of-autoclave manufacturing, thermal stability, etc.) might pave a way for future engineering and research applications in various sectors like aerospace or automotive industries especially when brake tools are taken into account while disadvantages like tooling costs and thickness limitations, which exist for thicker complex shapes due to the difficulty of achieving uniformity, should be taken into account.

Acknowledgements Authors are grateful to the Institute of Materials Science and Nanotechnology at Bilkent University. Furthermore, they thank Turkish Aerospace for supporting this presented research. In addition, authors thank M. Deveci, M. Özkutlu Demirel, F. Karaboğa, and E. Koştur for valuable discussions.

Funding Open access funding provided by the Scientific and Technological Research Council of Türkiye (TÜBİTAK). Authors acknowledge financial support by the Scientific and Technological Research Council of Turkey within the program 1515 with the number 5189901.

Declarations

Conflict of interest The authors declare no competing interests.

Open Access This article is licensed under a Creative Commons Attribution 4.0 International License, which permits use, sharing, adaptation, distribution and reproduction in any medium or format, as long as you give appropriate credit to the original author(s) and the source, provide a link to the Creative Commons licence, and indicate if changes were made. The images or other third party material in this article are included in the article's Creative Commons licence, unless indicated otherwise in a credit line to the material. If material is not included in the article's Creative Commons licence and your intended use is not permitted by statutory regulation or exceeds the permitted use, you will need to obtain permission directly from the copyright holder. To view a copy of this licence, visit <http://creativecommons.org/licenses/by/4.0/>.

References

- Kamali G, Ashokkumar N, Sugash K, Magesh V (2017) Advanced composite materials of the future in aerospace engineering. *Intl J Res Appl Sci Eng Technol* 5(2):610–614. <https://doi.org/10.22214/ijraset.2017.2091>
- Mrazova M (2013) Advanced composite materials of the future in aerospace industry. *INCAS Bulletin* 5(3):139–150. <https://doi.org/10.13111/2066-8201.2013.5.3.14>
- S. Rana, R. Figueiro. *Advanced composite materials for aerospace engineering*. Amsterdam: Elsevier, 2016. DOI: <https://doi.org/10.1016/C2014-0-00846-5>
- Marsh G (2007) Airbus takes on Boeing with reinforced plastic A350 XWB. *Reinf Plast* 51(11):26–29. [https://doi.org/10.1016/S0034-3617\(07\)70383-1](https://doi.org/10.1016/S0034-3617(07)70383-1)
- Marsh G (2011) Bombardier throws down the gauntlet with CSeries airliner. *Reinf Plast* 55(6):22–26. [https://doi.org/10.1016/S0034-3617\(11\)70181-3](https://doi.org/10.1016/S0034-3617(11)70181-3)
- Marinosci VM, Groupe WJB, de Rooij MB, Wijskamp S, Akkerman R (2021) Effect of grit-blasting on the fracture toughness of hybrid titanium-thermoplastic composite joints. *Int J Adhes Adhes* 109:102893. <https://doi.org/10.1016/j.ijadhadh.2021.102893>
- Tavakol B, Roozbehjavan P, Ahmed A, Das R, Joven R, Koushyar H, Rodriguez A, Minaie B (2013) Prediction of residual stresses and distortion in carbon fiber-epoxy composite parts due to curing process using finite element analysis. *J Appl Polym Sci* 128(2):941–950. <https://doi.org/10.1002/app.38075>
- Uhlmann E, Kersting R, Klein TB, Cruz MF, Borille AV (2015) Additive manufacturing of titanium alloy for aircraft components. *Procedia CIRP* 35:55–60. <https://doi.org/10.1016/j.procir.2015.08.061>
- Stichel T, Laumer T, Raths M, Roth S (2018) Multi-material deposition of polymer powders with vibrating nozzles for a new approach of laser sintering. *J Laser Micro/Nanoeng* 13(2):55–62. <https://doi.org/10.2961/jlmn.2018.02.0002>
- Öz Y, Yilmaz B, Evis Z (2022) A review on nanocomposites with graphene based fillers in poly(ether ether ketone). *Polym Sci, Ser A* 64(3):145–160. <https://doi.org/10.1134/S0965545X22030117>
- Cao D (2023) Fusion joining of thermoplastic composites with a carbon fabric heating element modified by multiwalled carbon nanotube sheets. *Intl J Adv Manuf Technol* 128(9):4443–4453. <https://doi.org/10.1007/s00170-023-12202-6>
- Cao D, Bouzolin D, Lu H, Griffith DT (2023) Bending and shear improvements in 3D-printed core sandwich composites through modification of resin uptake in the skin/core interphase region. *Compos B Eng* 264:110912. <https://doi.org/10.1016/j.compositesb.2023.110912>
- Cao D (2023) Investigation into surface-coated continuous flax fiber-reinforced natural sandwich composites via vacuum-assisted material extrusion. *Prog Addit Manuf*. <https://doi.org/10.1007/s40964-023-00508-6>
- Guo W, Hua L, Mao H, Meng Z (2012) Prediction of warpage in plastic injection molding based on design of experiments. *J Mech Sci Technol* 26(4):1133–1139. <https://doi.org/10.1007/s12206-012-0214-0>
- Bourell DL, Watt TJ, Leigh DK, Fulcher B (2014) Performance limitations in polymer laser sintering. *Phys Procedia* 56:147–156. <https://doi.org/10.1016/j.phpro.2014.08.157>
- Ghita O, James E, Davies R, Berretta S, Singh B, Flint S, Evans KE (2014) High temperature laser sintering (HT-LS): an investigation into mechanical properties and shrinkage characteristics of Poly (Ether Ketone) (PEK) structures. *Mater Des* 61:124–132. <https://doi.org/10.1016/j.matdes.2014.04.035>
- Guo N, Leu MC (2013) Additive manufacturing: technology, applications and research needs. *Front Mech Eng* 8(3):215–243. <https://doi.org/10.1007/s11465-013-0248-8>
- Wegner A, Witt G (2019) Adjustment of isotropic part properties in laser sintering based on adapted double laser exposure strategies. *Opt Laser Technol* 109:381–388. <https://doi.org/10.1016/j.optlastec.2018.08.017>
- Ageorges C, Ye L, Hou M (2001) Advances in fusion bonding techniques for joining thermoplastic matrix composites: a review. *Compos A Appl Sci Manuf* 32(6):839–857. [https://doi.org/10.1016/S1359-835X\(00\)00166-4](https://doi.org/10.1016/S1359-835X(00)00166-4)
- Iannone V, Barile M, Lecce L (2018) Automated fabrication of hybrid thermoplastic prepreg material to be processed by in-situ consolidation automated fiber placement process. *MATEC Web of Conferences* 188:01024. <https://doi.org/10.1051/mateconf/201818801024>
- Yavuz Z, Khaligh A, Öz Y, Tuncel D (2023) Effects of thermoplastic coating on interfacial interactions in advanced engineering composites for aerospace applications. *Polym Bull* <https://doi.org/10.1007/s00289-023-04807-4>
- B. Tijs, B. Veldman, A. Offringa. *Thermoplastic composites for primary aircraft structures: New trends in composite materials*. Workshop at the University of Girona, 2019.
- Pantelakis S, Tserpes K (2020) *Revolutionizing aircraft materials and processes*. New York: Springer Publishing. <https://doi.org/10.1007/978-3-030-35346-9>
- Arunkumar MP, Pitchaimani J, Gangadharan K, Babu MSL (2016) Sound transmission loss characteristics of sandwich aircraft panels: influence of nature of core. *J Sandwich Struct Mater* 19(1):26–48. <https://doi.org/10.1177/1099636216652580>
- Hu J, Li F, Wang B, Zhang H, Ji C, Wang S, Zhou Z (2020) A two-step combination strategy for significantly enhancing the interfacial adhesion of CF/PPS composites: The liquid-phase oxidation followed by grafting of silane coupling agent. *Compos B Eng* 191:107966. <https://doi.org/10.1016/j.compositesb.2020.107966>
- P Irving, C Soutis 2020 *Polymer composites in the aerospace industry*. Amsterdam: Elsevier <https://doi.org/10.1016/C2017-0-03502-4>
- Vasiliev VV, Barynin VA, Razin AF (2012) Anisogrid composite lattice structures – development and aerospace applications. *Compos Struct* 94(3):1117–1127. <https://doi.org/10.1016/j.compstruct.2011.10.023>
- H Pérez-Martín, P Mackenzie, A Baidak, CMÓ Brádaigh, D Ray, 2021 Crystallinity studies of PEKK and carbon fibre/PEKK composites: a review 223 109127 <https://doi.org/10.1016/j.compositesb.2021.109127>

29. Pérez-Martín H, Mackenzie P, Baidak A, Brádaigh CMÓ, Ray D (2022) Crystallisation behaviour and morphological studies of PEKK and carbon fibre/PEKK composites. *Compos A Appl Sci Manuf* 159:106992. <https://doi.org/10.1016/j.compositesa.2022.106992>
30. Danzi F, Campos PJS, Arteiro A, Dalli D, Furtado C, Chevalier J, Tavares RP, Lani F, Camanho PP (2023) Longitudinal failure mechanisms and crack resistance curves of unidirectional thermoplastic composites. *Eng Fract Mech* 282:109147. <https://doi.org/10.1016/j.engfracmech.2023.109147>
31. Ramaswamy K, Modi V, Rao PS, Martin PP, McCarthy CT, O'Higgins RM (2023) An investigation of the influence of matrix properties and fibre–matrix interface behaviour on the mechanical performance of carbon fibre-reinforced PEKK and PEEK composites. *Compos A Appl Sci Manuf* 165:107359. <https://doi.org/10.1016/j.compositesa.2022.107359>
32. El-Dessouky HM, Lawrence CA (2013) Ultra-lightweight carbon fibre/thermoplastic composite material using spread tow technology. *Compos B Eng* 50:91–97. <https://doi.org/10.1016/j.compositesb.2013.01.026>
33. Schledjewski R, Latrielle M (2003) Processing of unidirectional fiber reinforced tapes—fundamentals on the way to a process simulation tool (ProSimFRT). *Compos Sci Technol* 63(14):2111–2118. [https://doi.org/10.1016/S0266-3538\(03\)00108-8](https://doi.org/10.1016/S0266-3538(03)00108-8)
34. Atalay O, Öztürk F (2022) Effects of gripper location and blank geometry on the thermoforming of a composite sheet. *J Thermoplast Compos Mater* 36(7):2736–2757. <https://doi.org/10.1177/08927057221089830>
35. Faraj J, Pignon B, Baillieu J-L, Boyard N, Delaunay D, Orange G (2015) Heat transfer and crystallization modeling during compression molding of thermoplastic composite parts. *Key Eng Mater* 651–653:1507–1512. <https://doi.org/10.4028/www.scientific.net/KEM.651-653.1507>
36. Pilato LA, Michno MJ (1994) *Advanced composite materials*. New York: Springer Publishing. <https://doi.org/10.1007/978-3-662-35356-1>
37. Nakamura K, Katayama K, Amano T (1973) Some aspects of nonisothermal crystallization of polymers II Consideration of the isokinetic condition. *J Appl Polym Sci* 17(4):1031–1041. <https://doi.org/10.1002/app.1973.070170404>
38. Baran I, Cinar K, Ersoy N, Akkerman R, Hattel JH (2017) A review on the mechanical modeling of composite manufacturing processes. *Arch Comput Methods Eng* 24(2):365–395. <https://doi.org/10.1007/s11831-016-9167-2>
39. Long AC (2007) *Composite forming technologies*. Elsevier, Amsterdam
40. Gill P, Moghadam TT, Ranjbar B (2010) Differential Scanning Calorimetry Techniques: Applications in Biology and Nanoscience. *J Biomol Tech* 21(4):167–193
41. Wang H, Liu H, Ding Z, Li N (2021) Experimental and constitutive modelling studies of semicrystalline thermoplastics under solid-state stamp forming conditions. *Polymer* 228:123939. <https://doi.org/10.1016/j.polymer.2021.123939>
42. Lee K-I, Choe H-S, Kwak J-W, Lee J-S, Kweon J-H, Nam Y-W (2021) Evaluation of stamp forming process parameters for CF/PEKK thermoplastic composite using finite element method. *Kor Soc Compos Mater* 34(5):296–304. <https://doi.org/10.7234/composres.2021.34.5.296>
43. Chen H, Li S, Wang J, Ding A (2021) A focused review on the thermo-stamping process and simulation progresses of continuous fibre reinforced thermoplastic composites. *Compos B Eng* 224:109196. <https://doi.org/10.1016/j.compositesb.2021.109196>
44. Hu Y, Liao Y, Zheng Y, Ikeda K, Okabe R, Wu R, Ozaki R, Xu J, Xu Q (2022) Influence of cooling rate on crystallization behavior of semi-crystalline polypropylene: experiments and mathematical modeling. *Polymers* 14(17):3646. <https://doi.org/10.3390/polym14173646>
45. Tadini P, Grange N, Chetehouna K, Gascoïn N, Senave S, Reynaud I (2017) Thermal degradation analysis of innovative PEKK-based carbon composites for high-temperature aeronautical components. *Aerosp Sci Technol* 65:106–116. <https://doi.org/10.1016/j.ast.2017.02.011>
46. Huang B, Cheng S, Xi Q, Cai M (2012) Synthesis and characterization of novel copolymers of poly(ether ketone ketone) and poly(ether ketone sulfone imide). *Polym Bull* 69(6):661–673. <https://doi.org/10.1007/s00289-012-0753-7>
47. Wang P, Hamila N, Boisse P (2013) Thermoforming simulation of multilayer composites with continuous fibres and thermoplastic matrix. *Compos B Eng* 52:127–136. <https://doi.org/10.1016/j.compositesb.2013.03.045>
48. Habibi M, Darabi R, de Sa JC, Reis A (2021) An innovation in finite element simulation via crystal plasticity assessment of grain morphology effect on sheet metal formability. *Proc Instit Mech Eng Part L: J Mater : Des Appl* 235(8):1937–1951. <https://doi.org/10.1177/14644207211024686>
49. Dörr D, Brymerski W, Ropers S, Leutz D, Joppich T, Kärger L, Henning F (2017) A benchmark study of finite element codes for forming simulation of thermoplastic UD-tapes. *Procedia CIRP* 66:101–106. <https://doi.org/10.1016/j.procir.2017.03.223>

Publisher's Note Springer Nature remains neutral with regard to jurisdictional claims in published maps and institutional affiliations.